Quinazoline-based multi-tyrosine kinase inhibitors: Synthesis, modeling, antitumor and antiangiogenic properties

11 AUTHORS, INCLUDING:

Giovanni Marzaro
University of Padova
30 PUBLICATIONS **259** CITATIONS

SEE PROFILE

Rosa Di Liddo
University of Padova
55 PUBLICATIONS **787** CITATIONS

SEE PROFILE

Ignazio Castagliuolo
University of Padova
110 PUBLICATIONS **2,458** CITATIONS

SEE PROFILE

Adriana Chilin
University of Padova
89 PUBLICATIONS **764** CITATIONS

SEE PROFILE

Original article

Quinazoline-based multi-tyrosine kinase inhibitors: Synthesis, modeling, antitumor and antiangiogenic properties

Maria Teresa Conconi [a,1], Giovanni Marzaro [a,1], Luca Urbani [a], Ilenia Zanusso [a], Rosa Di Liddo [a], Ignazio Castagliuolo [b], Paola Brun [b], Francesca Tonus [a], Alessandro Ferrarese [a], Adriano Guiotto [a], Adriana Chilin [a,*]

[a] Department of Pharmaceutical and Pharmacological Sciences, University of Padova, Via Marzolo 5, 35131 Padova, Italy
[b] Department of Molecular Medicine, University of Padova, Via Gabelli 63, 35121 Padova, Italy

ARTICLE INFO

ABSTRACT

In this work the synthesis and the biological evaluation of some novel anilinoquinazoline derivatives carrying modifications in the quinazoline scaffold and in the aniline moiety were reported. Preliminary cytotoxicity studies identified three derivatives, carrying dioxygenated rings fused on the quinazoline portion and the biphenylamino substituent as aniline portion, as the most effective compounds. Further investigations revealed that these compounds exhibited antiproliferative activity on a wide panel of human tumor cell lines through the inhibition of both receptor and nonreceptor TKs. Furthermore, the compound bearing the dioxolane nucleus was also able to inhibit in vivo tumor growth. Molecular modeling of these compounds into kinase domain suggested that the phenyl group allows favorable interaction energies with the target proteins: this feature is favored by fused dioxygenated ring at the 6,7 positions, whereas free rotating functions do not allow the correct placement of the molecule, thus impairing the inhibitory potency. Finally, the biphenylamino derivatives, at noncytotoxic concentrations, acted as antiangiogenic agents both in in vitro and in vivo assays.

© 2013 Elsevier Masson SAS. All rights reserved.

1. Introduction

Alterations in cell cycle regulation may cause cancer onset, progression and metastasis [1]. Among the proteins involved in signal recognition, transduction and amplification, tyrosine kinases (TKs) play a key role [2,3]. These protein enzymes catalyze the transfer of a phosphate group from an ATP molecule to a tyrosine residue of the target protein, thus leading to signal transduction. Both receptor TKs (RTKs, such as EGFR, FGFR-1, VEGFR-1 and 2 and PDGFRβ) and cytoplasmic (or soluble) TKs (such as Src, Abl and Lck) have been to date discovered and characterized [4]. The RTKs are cell-surface receptors that are activated through the binding to specific growth factors, such as epidermal growth factor (EGF), insulin-like growth factor (IGF) and vascular endothelial growth factor (VEGF). In particular, the RTK activation causes receptor dimerization, phosphorylation of the proper substrate and then activation of the signal transduction cascade. Thus, the final effect of RTKs activation results in stimulation of cell growth and division [5]. In normal cells, TKs activity is tightly regulated to preserve the proper balance between proliferation and apoptosis. In almost all tumor tissues an overexpression or a gain-of-function mutations of several TKs have been detected [6,7]. Over the past two decades, the

strong efforts to develop useful strategies to inhibit TKs have allowed to identify inhibitors, such as small organic compounds (also known as TKs inhibitors, TKIs) and monoclonal antibodies (mAbs), that have been approved for therapy or have entered clinical trials [8]. The TKIs act as ATP-mimic inhibitors or growth factor binders, thus avoiding ATP binding. On the contrary, the mAbs act as growth factor-mimic inhibitors, so preventing the RTK activation.

Among the TKIs, 4-anilinoquinazolines have been intensively studied, leading to a number of active molecules already approved by FDA (e.g. erlotinib [9], gefitinib [10], lapatinib [11], vandetanib [12]) or under advanced clinical experimentation (e.g. afatinib [13], canertinib [14]). However, the development of novel analogs constitutes a field of great interest, as demonstrated by the number of patents filed and of the paper published in the last years [15]. Although the main target of 4-anilinoquinazoline is EGFR, some derivatives possess a poor selectivity profile targeting several kinases. For example, vandetanib is a dual EGFR/VEGFR-2 inhibitor, whereas afatinib and lapatinib target EGFR and Her2.

Continuing our studies in the field of quinazoline derivatives [16], herein we present the synthesis and the biological evaluation of some novel derivatives carrying modifications in the quinazoline scaffold and in the aniline moiety. These compounds have been initially screened for their cytotoxic activities against two cell lines, A431 (overexpressing EGFR) and NIH3T3 (not expressing EGFR). The most active compounds have been then submitted to in vitro assay on a panel of isolated TKs and molecular modeling studies have been carried out to figure out their interaction with TKs. Their effectiveness to inhibit in vivo tumor growth in a xenograft mouse model as well as their anti-angiogenic properties have been also evaluated.

2. Result and discussion

2.1. Chemistry

We planned to explore the effect of the different parts of the anilinoquinazoline nucleus on inhibition of cell proliferation, introducing some structural modifications in the quinazoline portion and in the aniline portion (Fig. 1).

The newly synthesized compounds were grouped in four series, according to the type of substituent in the quinazoline portion (Table 1) that were chosen on the basis of our previously reported work and on the analysis of the ATP binding pocket features in EGFR. In fact, the 6,7-fused dioxygenated rings (present in the A series) were found to improve the biological properties of the quinazoline derivatives [17]. On the other hand, the co-crystallized structure of EGFR with lapatinib (PDB ID: 1XKK) showed that the 6, 7 and 8 positions of quinazoline scaffold are surrounded by lipophilic residues (Leu718, from Leu792 to Cys797, Met1002; see Fig. S1 in Supplementary data). In particular Met793-Gly796 form a lipophilic cleft that could accommodate planar and lipophilic substituent, such as the allyloxy (see B series) or the phenyl (see D series) moieties. Moreover, Shen et al. have recently reported some monoalkylated imidazolinonequinazolines as EGFR inhibitors [18]. However, since no N,N-dialkylated imidazolinonequinazoline appeared in literature, we also considered the synthesis of the compounds, belonging to the C series. Preliminary molecular modeling studies were performed on compounds 10, 13 and 16 in order to evaluate in silico the effects of the different substitutions

on the quinazoline portion. All the compounds showed predicted binding poses comparable to the binding mode of lapatinib (see Fig. S2 in Supplementary data).

With respect to the aniline substituent, we considered both well known functionalization (as m-bromoaniline, m-toluidine and m-trifluoridine; see compounds 10–18) [19] as well as some previously unreported lipophilic functions (aminopicolines, m-methanesulphonamidoaniline, m-aminobiphenyl; see compounds 1–9). In fact it is well known that TKs present a deep lipophilic pocket accommodating the substituted aniline moiety [20].

All the compounds were prepared according to a common synthetic strategy (Scheme 1), that consisted in: 1) synthesis of the quinazoline nucleus, starting from the appropriate aniline derivatives, by the HMTA/TFA/K$_3$Fe(CN)$_6$ method [21]; 2) oxidation of the quinazoline nucleus to quinazolin-4(3H)-one by cerium ammonium nitrate (CAN) in aqueous acetic acid [22]; 3) chlorination at the 4 position with phosphorous oxychloride in the presence of triethylamine; 4) condensation of the 4-chloroquinazoline intermediates with the suitable substituted anilines. Compounds 1–4 were obtained as free bases, from chloroquinazolines and aminopicolines in the presence of sodium hydride in tetrahydrofuran, while compounds 5–18 were obtained directly as hydrochlorides irradiating the chloroquinazolines and the appropriate anilines in isopropanol, thus taking advantage of the microwave assisted organic chemistry technique.

The compounds of the A series were obtained from 8-chloro-[1,3]dioxolo[4,5-g]quinazoline (23a), 4-chloro-7,8-dihydro[1,4]dioxino[2,3-g]quinazoline (23b), and 4-chloro-8,9-dihydro-7H-[1,4]dioxepino[2,3-g]quinazoline (23c), previously described [16], which were condensed with 2-amino-4-picoline, 2-amino-6-picoline, 3-methansulfonamidoaniline or m-biphenylamine affording compounds 1–9.

For the compounds of the B series, the starting 3-allyloxy-4-methoxyaniline (19d) was prepared from 3-hydroxy-4-methoxynitrobenzene (24), which was condensed with allyl bromide in alkaline dimethylformamide to give the O-allylether 25, finally reduced with stannous chloride in ethanol to the desired 19d (Scheme 2).

The aniline intermediate 19e for the synthesis of compounds of the C series was synthesized starting from o-phenylendiamine (26), whose amino groups were protected as carbamates with ethyl chloroformate in tetrahydrofuran in the presence of triethylamine (Scheme 3). The N,N'-diprotected aniline 27 was nitrated with 65% nitric acid in acetic acid at reflux and the nitroderivative 28 was treated with methyl iodide in dimethylformamide in the presence of sodium hydride. Besides the desired methylation of the carbamic function, also the cyclization of the imidazolinone ring occurred. This unpredicted reaction probably proceeded through an initial N-monodeprotection with the formation of methylamine function, able to carry out a nucleophilic attack on the second carbamate group. The consequent elimination of ethanol furnished the desired compound. The nitroimidazolinone derivative 29 was finally submitted to reduction with stannous chloride in ethanol to achieve compound 19e.

For the synthesis of compounds of the D series, the benzo[h]quinazoline 21f was prepared starting from 6-bromobenzo[h]quinazoline (30) previously reported (Scheme 4) [23]. Debromination was accomplished by MW irradiation of compound 30 in the presence of sodium ethylate in ethanol.

2.2. Biology

2.2.1. In vitro screening of synthesized compounds

The compounds listed in Table 1 were screened for their antiproliferative effects on two cell lines: A431 cells and NIH3T3 cells,
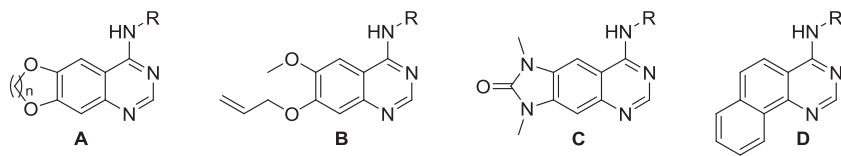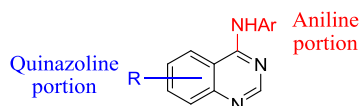

Fig. 1. Points of modifications in the anilinoquinazoline nucleus.
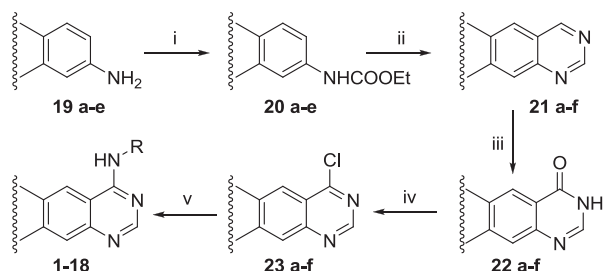
Table 1
Structures of title compounds.

Compound	Series	n	R	Compound	Series	n	R
1	A	1	pyridinyl–CH$_3$	**10**	B	–	phenyl–Br
2	A	2	pyridinyl–CH$_3$	**11**	B	–	phenyl–CH$_3$
3	A	1	pyridinyl–CH$_3$	**12**	B	–	phenyl–CF$_3$
4	A	2	pyridinyl–CH$_3$	**13**	C	–	phenyl–Br
5	A	1	phenyl–NHSO$_2$CH$_3$	**14**	C	–	phenyl–CH$_3$
6	A	2	phenyl–NHSO$_2$CH$_3$	**15**	C	–	phenyl–CF$_3$
7	A	1	biphenyl	**16**	D	–	phenyl–Br
8	A	2	biphenyl	**17**	D	–	phenyl–CH$_3$
9	A	3	biphenyl	**18**	D	–	phenyl–CF$_3$

that over-express or lack EGFR, respectively. PD153035, one of the most potent EGFR inhibitor (IC$_{50}$ = 25pM) [24] sharing with the novel compounds the aminoquinazoline moiety, was used as reference. The inhibitory effects on cell proliferation were determined by MTT assay (Table 2). The compounds belonging to the C and D series were almost ineffective on both cell lines, while the 7-allyloxy derivatives **10**, **11**, and **12**, bearing methoxy and allyloxy groups in the 6 and 7 positions respectively of the quinazoline nucleus, showed IC$_{50}$ values against A431 cells comparable to

Scheme 1. General strategy for the synthesis of quinazoline derivatives. *Reagent and conditions*: (i) ClCOOEt, TEA, THF, rt, 30 min; (ii) 1. HMTA, TFA, MW, 110 °C, 10 min. 2. K$_3$Fe(CN)$_6$, KOH 10%, EtOH/H$_2$O 1/1, reflux, 4 h; (iii) CAN, AcOH, H$_2$O, rt, 5 min; (iv) POCl$_3$, TEA, reflux, 3 h; (v) RNH$_2$, NaH, THF, 1 h (for cpds **1**–**4**) or RNH$_2$, *i*-PrOH, MW, 80 °C, 15–30 min (for cpds **5**–**18**). Letter specifications: **a** = dioxolane derivatives; **b** = dioxano derivatives; **c** = dioxepino derivatives; **d** = allyloxy derivatives; **e** = imidazolinone derivatives; **f** = benzoquinazoline derivatives. See Table 1 for R specification.
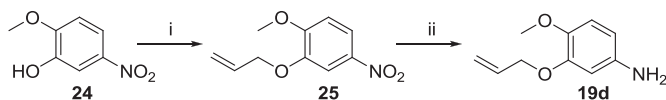
PD153035 and to our previously reported compounds carrying a dioxolane or dioxepine rings condensed on the quinazoline portion [16]. In the A series, compound **2** showed an inhibitory activity comparable to that of the reference compound, whereas compounds **1**, **3**, **4**, **5** and **6** seemed to be ineffective. On the contrary, derivatives **7**–**9**, carrying dioxygenated rings fused on the quinazoline portion and the biphenylamino substituent as aniline portion, exhibited a very strong antiproliferative activity, their IC$_{50}$ values being about 5–50 times lower than that determined for PD153035. Furthermore, the dioxane derivative was more effective than the corresponding dioxolane and dioxepine derivatives, in agreement with our previous findings [16,17].

Interestingly, the biphenyl derivatives exhibited cytotoxic effects also in NIH3T3 cells lacking EGFR. IC$_{50}$ values for compounds **7** and **9** were quite similar to those determined in A431 cells. Although antiproliferative activity of compound **8** seemed to be lower in NIH3T3 cells respect to A431 ones, the corresponding IC$_{50}$ value was comparable to those detected for compounds **7** and **9**. The maintenance of cytotoxic activity on NIH3T3 cells suggested that these compounds could exert their effects by interacting with additional cell target, other than EGFR. Since all eukaryotic tyrosine kinases share a conserved catalytic domain able to transfer the phosphate group of ATP to aminoacid residues on protein substrates [20], we have hypothesized that the above mentioned compounds could act as multi-TKIs.
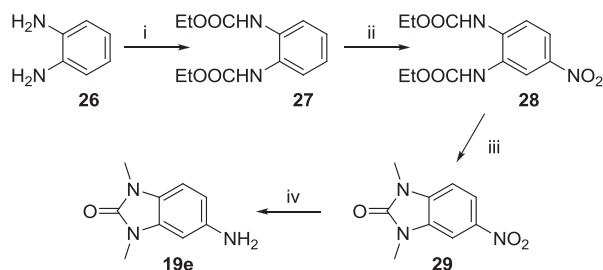
To verify this hypothesis, compounds **7**–**9** were tested against a panel of both receptor (EGFR, FGFR-1, VEGFR and PDGFRβ) and

Scheme 2. Synthesis of the aniline intermediate **19d**. *Reagent and conditions*: (i) allyl bromide, K_2CO_3, DMF, reflux, 16 h; (ii) $SnCl_2 \cdot 2H_2O$, EtOH, reflux, 6 h.

Scheme 3. Synthesis of the aniline intermediate **19e**. *Reagent and conditions*: (i) ClCOOEt, TEA, THF, rt, 1 h; (ii) 65% HNO_3, AcOH, reflux, 1 h; (iii) MeI, NaH, DMF, rt, 10 min; (iv) $SnCl_2 \cdot 2H_2O$, EtOH, reflux, 6 h.

soluble (Abl1 and Src) TKs. All the derivatives were found to possess a broad inhibitory activity (Table 3) although they hindered RTKs and soluble TKs at different extents. In particular, the dioxolane derivative **7** seemed to be the most effective, showing IC_{50} values at sub-micromolar concentrations on all tested TKs.

2.2.2. Effects of compounds 7–9 on cancer cell lines and in vivo tumor growth

Since the three biphenyl derivatives appeared the most promising compounds, further investigations were performed on a panel of human tumor cell lines derived from breast (MCF-7) and colon (HT-29) adenocarcinomas, cervical cancer (HeLa), and on the murine hepatocellular carcinoma cell line BNL (BNL 1 ME A.7R.1). Overall, in MCF-7, HT-29, and HeLa cells, compounds **7**–**9** presented IC_{50} values about 6–10 times lower than those determined for PD153035, except for compound **9** showing an antiproliferative activity in Hela cells comparable to reference compound (Table 4). Furthermore, also in the BNL cells all compounds showed a comparable activity and inhibited cell proliferation to the same degree of PD153035.

We next determined whether the compounds inhibited tumor growth in a typical transplanted model of syngenic hepatocellular carcinoma in Balb/c mice. As reported in Fig. 2, daily intraperitoneal administration of 50 mg/kg of compound **7** significantly reduced tumor growth as compared to not treated animals whereas compound **8** did not achieve a statistical difference in tumor growth. Administration of compound **9** caused severe body weight loss in animals therefore they were suppressed after 3 days of treatment.

2.2.3. Antiangiogenic properties of compounds 7–9

Tumor development and maintenance require a permissive microenvironment. In the absence of new blood vessel formation the cancer can't grow over a volume of 1–2 mm³ [25]. As a consequence of cell hypoxia, several pro-angiogenic factors, such as basic
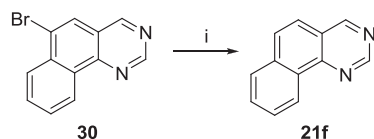
Scheme 4. Synthesis of benzo[*h*]quinazoline **21f**. *Reagent and conditions*: (i) EtONa, EtOH, MW, 105 °C, 15 min.

Table 2
IC_{50} values for 72 h exposure of cells to the compounds.

Compound	IC_{50} (μM)[a] against cell lines	
	A431	NH3T3
1	>10[b]	>10[b]
2	5.17 ± 0.84	6.60 ± 1.07
3	>10[b]	>10[b]
4	>10[b]	>10[b]
5	>10[b]	>10[b]
6	>10[b]	>10[b]
7	0.81 ± 0.06	0.60 ± 0.02
8	0.08 ± 0.01	0.60 ± 0.20
9	0.66 ± 0.08	0.92 ± 0.06
10	4.49 ± 0.62	>10[b]
11	8.45 ± 0.55	6.60 ± 0.70
12	5.95 ± 0.01	>10[b]
13	>10[b]	>10[b]
14	>10[b]	>10[b]
15	>10[b]	>10[b]
16	>10[b]	>10[b]
17	>10[b]	>10[b]
18	>10[b]	>10[b]
PD153035	4.40 ± 1.30	>10[b]

[a] The values are the mean ± SD of at least three independent experiments.
[b] IC_{50} not determined because less than 50% inhibition was observed at the highest tested concentration (10 μM). Higher concentrations were not used to avoid precipitation of the compounds in the culture medium.

Fibroblast Growth Factor (bFGF), Platelet Derived Growth Factor (PDGF), VEGF and EGF, are released thus inducing the angiogenesis process that in turn creates the basic conditions for cancer growth and metastasis [26,27]. The binding between these factors and the TKs leads the cells to enter in G2/M phases and also inhibits apoptosis processes. Thus, the endothelial cell (EC) growth rate is dramatically accelerated, happening as rapidly as every few days, whereas under physiological conditions ECs divide every years [28]. In the last years great attention has been paid to the angiogenesis for the development of novel anticancer targeted therapies.

Our data demonstrated that compounds **7**–**9** are able to inhibit the phosphorylation of some TKs involved in the formation of new blood vessels. VEGF-A and VEGFR-2 are currently the main targets for anti-angiogenic efforts [29]. Together with FGF and its receptor, they are overexpressed in different types of tumors and their signaling promotes the proliferation, migration, and differentiation of vascular ECs [30]. PDGFRβ and its ligands induce vessel maturation and the recruitment of pericytes [31]. On the other hand, EGFR pathway acts as an indirect regulator of angiogenesis because its activation stimulates the production of pro-angiogenic factors, such as VEGF.34 Nonreceptor TKs, namely Src and Abl1, can be activated also by growth factors through receptor TKs, like EGFR, PDGFRβ, FGFR and VEGFR, leading to an increased expression of proangiogenic cytokines [32–36].

Starting from these considerations, it seemed noteworthy to verify whether the most active compounds, that is the biphenyl derivatives **7**–**9**, could affect the angiogenic process. The effects of these compounds on the proliferation, migration and tube formation of human umbilical vein cord cells (HUVECs) have been *in vitro* verified, thus mimicking the various steps of new blood vessels formation [17]. The biphenyl derivatives presented IC_{50} values lower than that determined for PD153035, as shown in Table 4, and in particular compound **8** was much more cytotoxic than compounds **7** and **9**.

The antiproliferative activity seemed to be due to a pro-apoptotic effect. Indeed, after a 24 h incubation period, all compounds (10 μM), except for compound **7**, induced significant decreases in cell proliferation (Fig. 3a) and increases in the apoptotic rate (Fig. 3b) when compared to not treated cultured.

Table 3
Kinase inhibition profile of the compounds.[a]

Compounds	IC$_{50}$ (μM) or % inhibition ([I] = 1 μM) against isolated kinases					
	EGFR	FGFR-1	VEGFR-2	PDGFRβ	Src	Abl
7	0.002 ± 0.001	0.063 ± 0.015	0.848 ± 0.110	0.243 ± 0.056	0.032 ± 0.008	0.051 ± 0.010
8	20%	0.178 ± 0.030	50%	0.100 ± 0.045	0.642 ± 0.105	0.024 ± 0.010
9	0.027 ± 0.012	0.063 ± 0.025	30%	40%	0.645 ± 0.085	0.056 ± 0.016

[a] The values represent the mean ± SD of at least three independent experiments.

To avoid direct cytotoxic effects, migration and morphogenesis assays were carried out treating cultures with the highest not cytotoxic concentrations of the tested compounds, as determined from MTT assay (data not shown). Cell migration was significantly decreased by 1 μM PD153035 and biphenyl derivatives (Fig. 4a). After 18 h from seeding on Matrigel, HUVECs gave rise to tubule-like structures (Fig. 4b) that was disrupted by incubation with compound **8** (Fig. 4c). Image analysis confirmed these observation, showing that compound **8** significantly decreased both dimensional and topological parameters (Fig. 4d). On the other hand, PD153035 and other compounds affected only the number of meshes. The inhibitory effect on in vitro angiogenesis was achieved using compound concentration not affecting cell proliferation and viability. To date, the main side effects of TKIs target the cardiovascular system, and are in part related to direct effects on normal ECs. Although most normal blood vessels remain quiescent, however growth factor signaling maintains EC survival and vascular integrity. Thus, cardiovascular toxicity may be a consequence of an impaired EC renewal capacity [37]. The maintenance of HUVEC viability in the presence of compound concentration able to induce anti-angiogenic effects may suggest a reduced toxicity of biphenyl derivatives.

To verify in vivo the anti-angiogenic activity of compounds, Matrigel plugs containing FGF-2 (200 ng/plug) alone or with the compounds (1 μM) were implanted subcutaneously into the flank of C57/BL6 mice. The mean hemoglobin concentration in compound-treated Matrigel plugs was significantly lower than FGF-2-treated Matrigel plugs, but higher than that determined in control. The reference compound was unable to inhibit the FGF-2-induced neovascularization (Fig. 4e).

2.3. Synthesis of analogs of compounds 7–9 and molecular modeling

On the basis of the above described results and to deeply investigate the role of the biphenylamino function in the anti-TKs activity, we synthesized some "hybrid" compounds bearing this substituent on the quinazoline scaffold of known tyrosine kinase inhibitors, such as PD153035, erlotinib and gefitinib. The hybrid compounds **34**–**36** were synthesized according to the same synthetic route described in Scheme 1, starting from the opportune 4-chloroquinazoline intermediates **31**–**33** already reported (Scheme 5) [22].

The compounds **34**, **35**, and **36** exerted poor antiproliferative activity on A431 and NIH3T3 cells: 10 μM compounds induced about 70% reduction in cell number respect to that determined in untreated cultures. Similarly, the three novel compounds were unable to counteract the kinase activity of EGFR, FGFR-1, VEGFR-2, PDGFRβ, Abl1 and Src (IC$_{50}$ higher than 1 μM in all the cases).

Thus, we concluded that the remarkable biological properties of compounds **7**–**9** derived from the presence of both the fused dioxygenated ring and the biphenylamino moiety. To rationalize this behavior, molecular modeling studies were performed. Compounds **7** and **34** were docked in the DFG-out crystallographic structure of EGFR, FGFR-1, VEGFR-2, Src and Abl1 (PDB IDs: 1XKK, 3C4F, 3EWH, 3EN6, 2QOH respectively). The visual inspection of the binding poses revealed that the terminal phenyl ring of compound **7** was able to establish "edge-to-face" arene–arene interactions with the phenylalanine of the DFG-motif of EGFR, FGFR-1, Abl1 and Src (Fig. 5a–d). On the contrary, the DFG-motif of VEGFR-2 was not involved in the interaction (Fig. 5e). This observation is consistent with the data reported in Table 3: the IC$_{50}$ against VEGFR-2 was bout 15–400 times higher than the IC$_{50}$ against the other TKs considered in the docking studies.

In the case of compound **34** the molecular docking studies revealed that the steric hindrance generated by the bulkier free-rotating methoxy functions caused a rotation of the quinazoline scaffold of **34** in order to maintain the correct placement of the biphenyl function. This feature determines a larger distance between Met793 and the quinazoline nitrogen of compound **34** in comparison with that of compound 7 (Fig. 5f–h). This was detrimental for the formation of the H-bond between the quinazoline nucleus and the protein backbone (that is known to be fundamental [20]), thus causing a dramatic decrease in the ability to counteract the kinase activity.

3. Conclusions

In this work the synthesis and biological evaluation of four classes of aminoquinazoline derivatives have been reported. Taken together, our results indicate that the functionalization of the aniline moiety with a further benzene ring together with dioxygenated rings fused to quinazoline core lead to compounds (**7**, **8**, and **9**) characterized by high antiproliferative activity through the inhibition of a wide panel of both receptor and nonreceptor TKs.

Table 4
IC$_{50}$ values for 72 h exposure of tumor cell lines and HUVECs to the compounds.

Compounds	IC$_{50}$ (μM)[a] against cell lines						
	A431	NIH3T3	MCF-7β	HT-29	HeLa	BNL	HUVEC
7	0.81 ± 0.06	0.61 ± 0.02	0.77 ± 0.02	0.95 ± 0.06	0.77 ± 0.02	2.80 ± 0.65	0.75 ± 0.01
8	0.08 ± 0.01	0.60 ± 0.20	0.74 ± 0.06	0.68 ± 0.36	0.62 ± 0.01	2.70 ± 0.35	0.08 ± 0.01
9	0.66 ± 0.08	0.92 ± 0.06	0.70 ± 0.11	0.71 ± 0.01	5.49 ± 0.62	3.00 ± 0.80	0.91 ± 0.06
PD153035	4.42 ± 1.29	>10[b]	8.21 ± 0.71	>10[b]	>10[b]	9.50 ± 0.40	4.06 ± 0.19

[a] The values are the mean ± SD of at least three independent experiments.
[b] IC$_{50}$ not determined because less than 50% inhibition was observed at the highest tested concentration (10 μM). Higher concentrations were not used to avoid precipitation of the compounds in the culture medium.
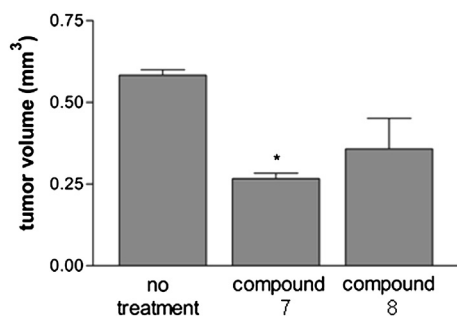
Fig. 2. Inhibition of tumor growth *in vivo* by compounds **7** and **8**. Male mice were injected subcutaneously with a syngenic hepatocellular carcinoma cell line, BNL 1ME A.7R.1 cells. Tumor-bearing mice were injected daily i.p. with vehicle as a control or 50 mg/kg of compound **7** or **8**. The figure shows the average measured tumor volumes after 7 days of treatment. Data are presented as the mean ± SEM of tumor volume for five animals per group. *$p < 0.05$ vs control.

Molecular modeling of these compounds into kinase domain has suggested that the phenyl group allows favorable interaction energies with the target proteins and that this feature is favored by the reduced steric hindrance of the fused dioxygenated ring at the 6,7 positions with respect to different alkoxy functions. Among the biphenyl derivatives, compound **7**, bearing the dioxolane nucleus, has been shown to significantly reduce *in vivo* tumor growth. Interestingly, compounds **7**–**9**, at noncytotoxic concentrations, exerted also anti-angiogenic effects both *in vitro* and *in vivo* assays. Thus, we can suppose that they may affect neo-vessel formation without impairing the viability of ECs, leading then to reduced potential cardiovascular side effects. This hypothesis will be verified by further *in vivo* investigations. In conclusion, our findings indicate that the biphenyl derivatives, acting as multi-kinase inhibitor, may possess therapeutic potential for cancer treatment.

4. Experimental section

4.1. Chemistry

See Supplementary data for general synthetic methods, for the synthesis of **19d**–**e**, **21f**, **25**, **27**, **28**, **29** and for the analytical details (mp, NMR, HRMS, elemental analyses) of all compounds. Compounds **19a**–**c** [16], **20a**–**c** [16], **21a**–**c** [16], **22a**–**c** [16], **23a**–**c** [16], **30** [23], **31**–**33** [22] were synthesized as previously reported. Compounds **24**, **26** and all the anilines used for the final condensation were commercially available.

4.1.1. General procedure for carbamates 20d–e

A mixture of aniline (**19d**–**e**) (13.0 mmol), ethyl chloroformate (2.5 mL, 26.0 mmol) and Et_3N (3.6 mL, 26.0 mmol) in anhydrous THF (150 mL) was stirred at room temperature for 30 min. The solid was filtered off and the solvent was evaporated under reduced pressure. The residue was dissolved in CH_2Cl_2 (100 mL) and the organic layer was washed with water (3 × 50 mL). The organic phase was evaporated under reduced pressure to give **20d**–**e** in quantitative yield (98%).

4.1.2. General procedure for quinazolines 21d–e

A mixture of ethyl carbamate (**20d**–**e**) (10.0 mmol) and hexamethylenetetramine (1.4 g, 10.0 mmol) in TFA (30 mL) was microwave irradiated at 110 °C (power set point 80 W; ramp time 1 min; hold time 10 min). After cooling the mixture was diluted with aqueous ethanolic (water/EtOH: 1/1) 10% KOH (300 mL), added with $K_3Fe(CN)_6$ (26.3 g, 80.0 mmol) and stirred to reflux for 4 h. After cooling the mixture was diluted with water (300 mL) and extracted with CH_2Cl_2 (3 × 200 mL). The organic phase was evaporated under reduced pressure to give the quinazoline **21d**–**e** (yields 40–91%).

4.1.3. General procedure for quinazolin-4(3H)-ones 22d–f

To a solution of quinazoline (**21d**–**f**) (5.0 mmol) in AcOH (2.0 mL) a solution of CAN (10.8 g, 20.0 mmol) in water (10 mL) was added dropwise. A white precipitate was formed, which was collected by filtration affording compounds **22d**–**f** (yields 43–98%).

4.1.4. General procedure for 4-chloroquinazolines 23d–f

A suspension of quinazolinone (**22d**–**f**) (2.0 mmol) in $POCl_3$ (4.0 mL) and TEA (1.0 mL) was heated to reflux for 3 h. After cooling the mixture was concentrated under reduced pressure and the solid residue was dissolved in EtOAc (50 mL) and washed with sat. $NaHCO_3$ solution (2 × 20 mL). The organic phase was evaporated under reduced pressure affording compounds **23d**–**f** (yields 63–93%).

4.1.5. General procedure for 4-pyridylaminoquinazolines 1–4

To a solution of 4-chloroquinazoline **23a** [16] or **23b** [16] (0.5 mmol) in THF (4 mL), 2-amino-4-picoline or 2-amino-6-picoline (60 mg, 0.6 mmol) and NaH (60 mg, 2.5 mmol) were added. The mixture was stirred at room temperature for 5 min and then refluxed for 1.5 h. After cooling the mixture was poured in water (5 mL) and the precipitate was collected by filtration to give the title compounds (yields 15–75%).
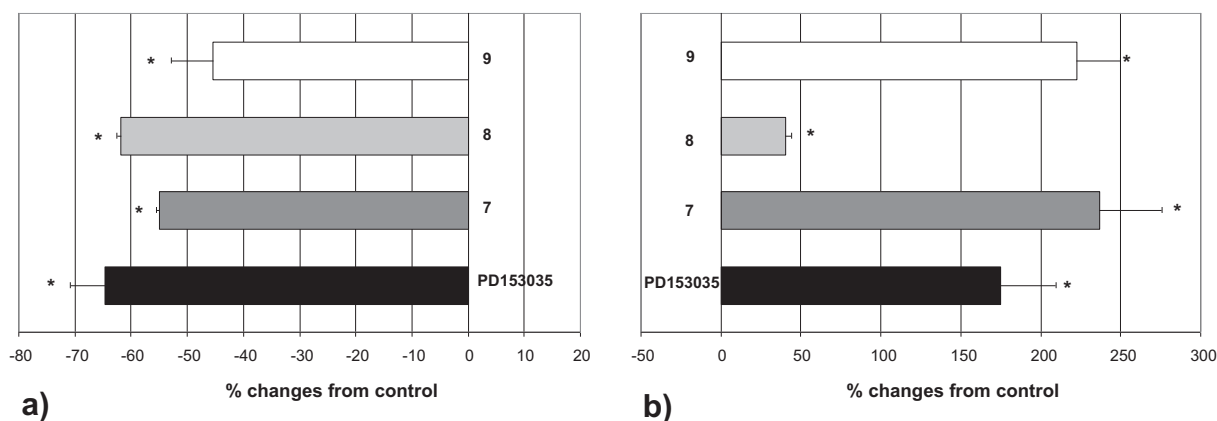

Fig. 3. Pro-apoptotic effects of compounds on HUVECs. After a 24 h incubation period with compounds (10 μM), both cell viability (a) and apoptotic rate (b) were determined by MTT assay and assessment of mono- and oligo-nucleosomes formation, respectively. Results, expressed as percent change from control cultures (taken as 0), are the mean ± SD of at least three independent experiments. * =$p < 0.05$ vs control cultures, Student *t* test.
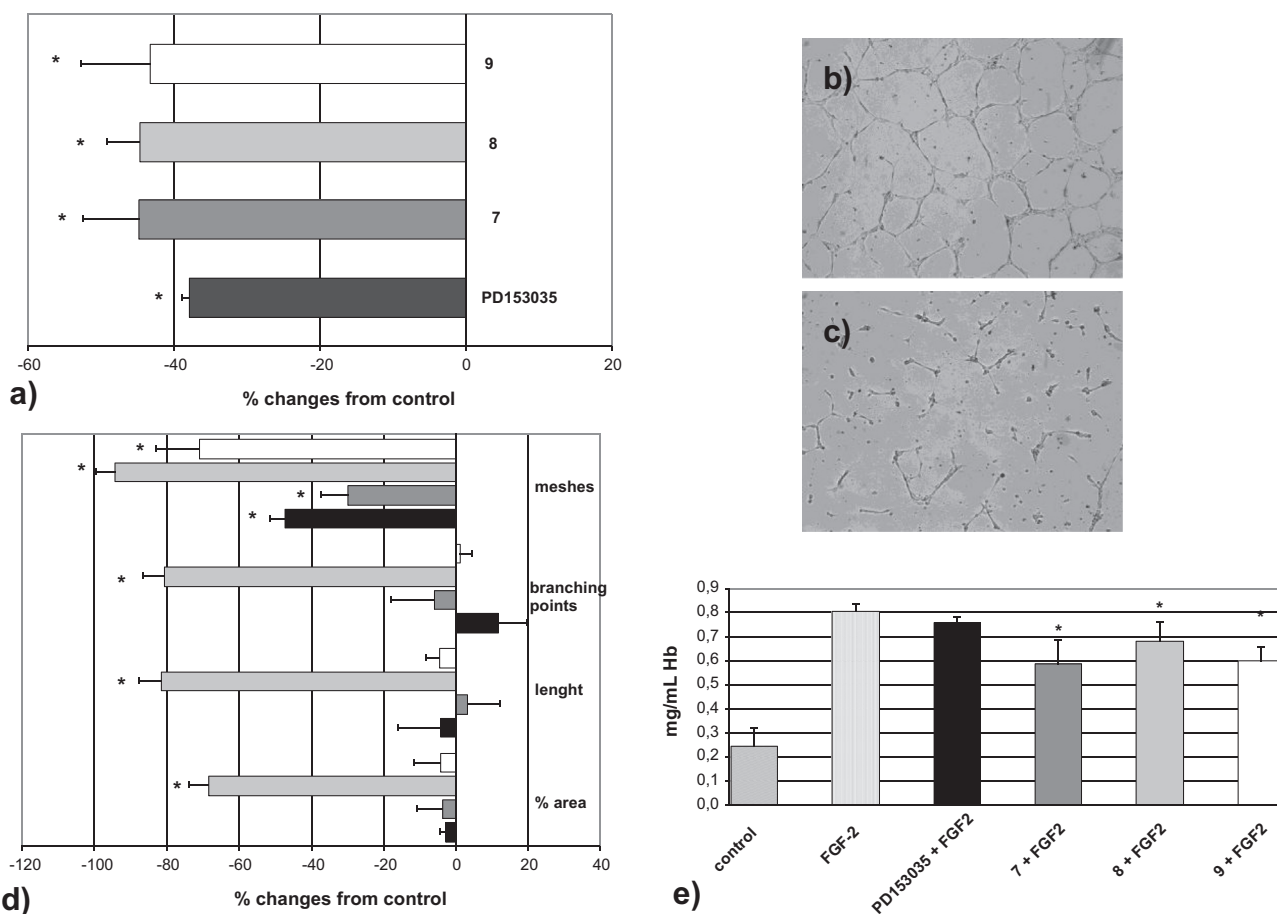
Fig. 4. Effects on *in vitro* and *in vivo* angiogenesis. For the *in vitro* experiments, cells were treated with compounds at the highest concentration not inducing decrease in cell viability (1 and 0.1 µM for migration and morphogenesis assays, respectively). Bars are means ± S.D. of three separate experiments. * $= p < 0.05$ vs control cultures, Student t test. a): HUVEC migration through a 5.0 µm pore after 4 h from seeding. Results are expressed as percent change from control not treated cultures (taken as 0). Phase contrast micrographs of HUVEC cultures on Matrigel nontreated (b) or incubated with 0.1 µM compound **8** (c). d): Quantitative analysis of the effects of compounds on the dimensional (percent area covered by HUVECs and total length per field), and topological parameters (number of branching points per field, number of mesh per field and percent area inside meshes) of the HUVEC meshwork. Bars: black, PD153035; dark gray, compound **7**; light gray, compound **8**; white, compound **9**. e): Quantitative hemoglobin (Hb) content in the Matrigel plug was determined using the Drabkin's Reagent kit.

### 4.1.6. General procedure for 4-anilinoquinazolines 5–18, 34–36

A mixture of 4-chloroquinazoline (**23a–c** [16], **23d–f**, **31–33** [22]) (0.5 mmol) and the appropriate aniline (0.5 mmol) in *i*-PrOH (1 mL) was microwave irradiated at 80 °C (power set point 60 W; ramp time 1 min; hold time 15 min). After cooling, the obtained precipitate was collected by filtration to give compounds **5–18** and **33–35** as hydrochlorides (yields 52–93%).

4.2. Computational methodology

All the computational studies were carried out on a 4 CPUs (Inteol Core2 Quad CPU Q9550 @ 2.83 GHz) ACPI x64 Linux work-station with Ubuntu 12.04 operating system. All X-ray structure data of EGFR, VEGFR-2, FGFR-1, Src and Abl1 have been downloaded from Protein Data Bank (PDB) and have been analyzed and handled with Chimera 1.5.3 software [38]. The structure of compounds **7**, **10**, **13**, **16** and **34** has been prepared using MarvinSketch 5.5.0.1 software [39]. The lowest energy conformations were determined at pH 7.4 with OpenBabel 2.2.3 software [40], using the MMFF94s force field. All docking studies have been performed with AutoDock 4.2 software, employing AutoDock Tools (ADT) 1.5.4 graphical interface [41]. For the ligands, the Gasteiger charges were computed and the nonpolar hydrogen atoms were merged with ADT, thus preparing the appropriate PDBQT files for the molecular docking studies.

Each crystallographic complex of the TKs in complex with inhibitors (1XKK for EGFR, 3EWH for VEGFR-2, 3C4F for FGFR-1, 3EN6 for Src and 2QOH for Abl1) has been initially independently loaded in Chimera software. PDGFRß was not considered since the crystallographic structure of the kinase domain has not yet been resolved. The water molecules, the co-factors and the ligand were
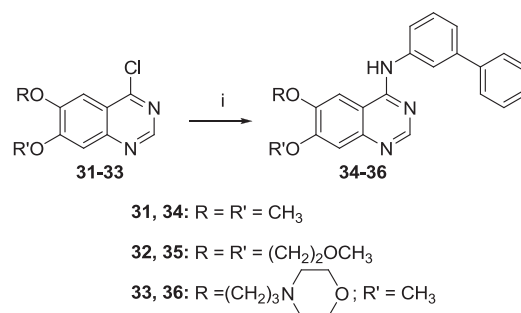
Scheme 5. Synthesis of quinazoline derivatives **34** (PD153035-like), **35** (erlotinib-like) and **36** (gefitinib-like). *Reagent and conditions*: (i) 3-aminobiphenyl, *i*-PrOH, MW, 80 °C, 15 min.
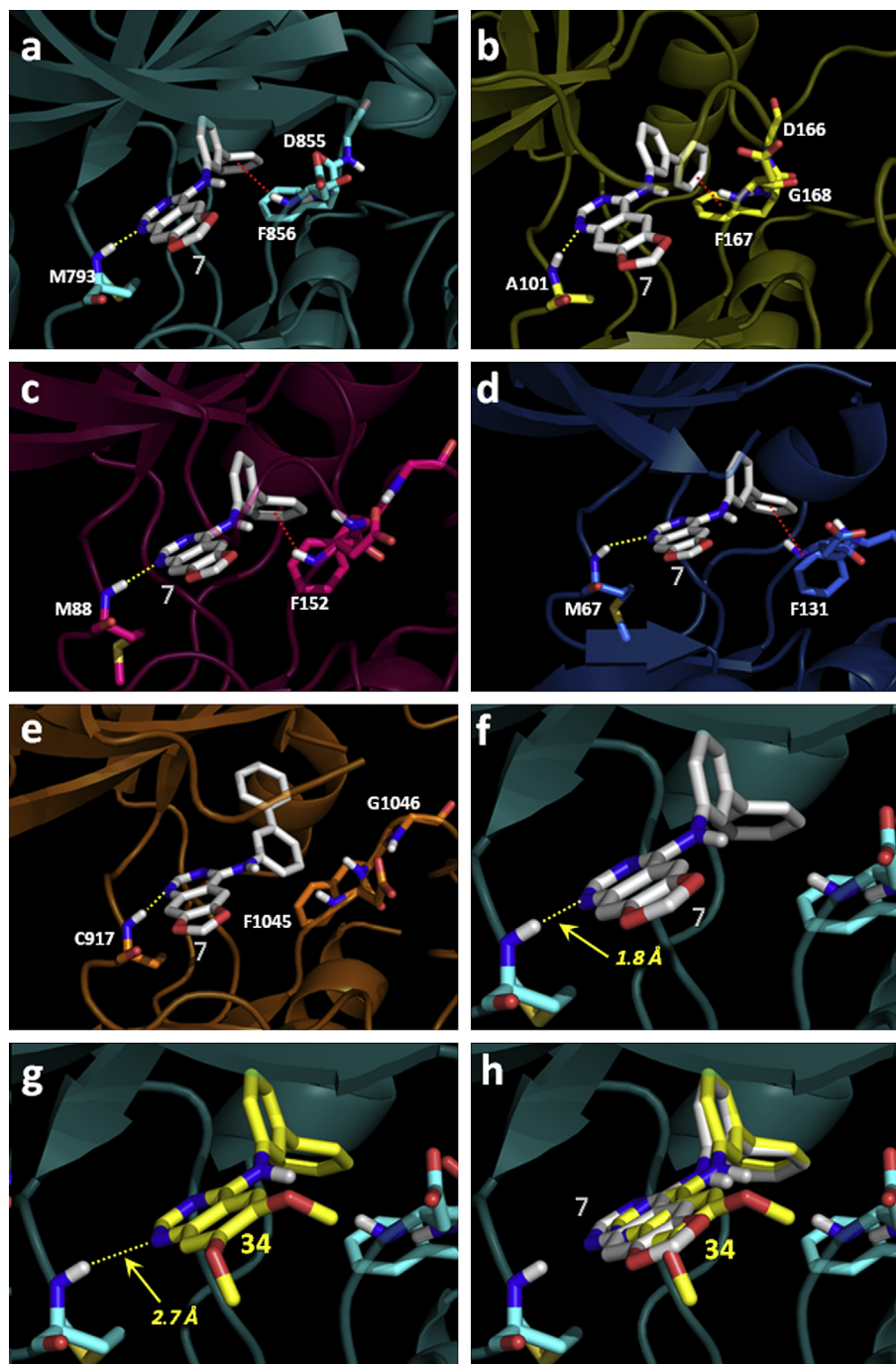
Fig. 5. Binding modes predicted for compound **7** in EGFR (a), FGFR1 (b), Abl1 (c), Src (d), VEGFR-2 (e); details of the distance between Met793 and the quinazoline nitrogen for compound **7** (f) and for compound **34** (g); superimposition of the binding modes for the two ligands (h). Note the difference in the quinazoline scaffold placement due to steric hindrance generated by the two methoxylic functions.

removed. The handled protein structure was then saved as PDB file and loaded in ADT software. The hydrogen atoms were added and the Gasteiger charges were computed. After the addition of the AutoDock atom types the nonpolar hydrogen atoms were merged and the protein was saved in PDBQT format required for AutoDock to work. AutoDock makes use of two packages, AutoGrid (that computes several atom-specific grids) and AutoDock (that performs the conformational analysis based on the pre-calculated grids). In all cases, the grids have been calculated using following parameter settings: atom types = A, C, N, NA, OA; center of the grids on the center of the co-crystallized ligand; number of point on *x*, *y*

and *z*-dimensions = 60; spacing = 0.375 Å (the resulting grids were thus computed in a cube with sides of 22.5 Å). The conformational searches have been performed setting the default parameters for Lamarckian Genetic Algorithm search method.

4.3. Biology

4.3.1. In vitro kinase assays

Novel compounds were tested *in vitro* for inhibition of selected TKs. Recombinant EGFR (Invitrogen, Milan, Italy), FGFR-1 and VEGFR-2 (purchased from Sigma, Milan, Italy) were diluted in kinase

dilution buffer (5 mM MOPS pH 7.2, 2.5 mM glycerol 2-phosphate, 5 mM MgCl2, 0.4 mM EGTA, 0.4 mM EDTA, 0.05 mM DTT, 0.5 mM BSA). Active kinases (final concentration 200 ng/mL) were added to compounds at concentrations ranging from 1 μM to 0.01 μM. The final reaction mixture (25 μL), prepared in pre-cooled micro-centrifuge tubes, contained 0.2 mg/ml substrate solution (Myelin Basic Protein, MBP, Sigma), 0.05 mM ATP and 0.25 μCi of $[\gamma\text{-}^{32}P]ATP$ (PerkinElmer, Monza, MI). Negative controls were prepared replacing the substrate solution with water whereas positive controls were set up replacing inhibitors tested with water. Reactions were carried out at 30 °C for 20 min and stopped by addition of loading buffer containing 0.25 mM β-mercaptoethanol. Samples were then subjected to electrophoresis on 10% w/v SDS-PAGE gel. Gels were dried, and phosphorylated myelin basic protein was identified by autoradiography. The VersaDoc Quantity One software (BioRad) was used for densitometric analysis. Results were expressed as IC_{50} (μM) or % inhibition ([I] = 1 μM) against purified kinases.

4.3.2. Cell culture

A431 human vulvar squamous carcinoma cells overexpressing HER-1 [42] and NIH3T3 murine embryonic fibroblast-like cells lacking EGF receptors [42], human colonic adenocarcinoma HT-29 and murine hepatocarcinoma BNL 1ME A.7R.1 were purchased by Istituto Zooprofilattico Sperimentale della Lombardia e dell'Emilia-Romagna (Brescia, Italy), whereas human MCF-7 and HeLa were obtained from American Tissue Culture Collection (ATCC, Manassas, Virginia). A431, HT-29, HeLa, MCF-7, and BNL cell lines were grown in monolayer culture with DMEM High Glucose medium (Euroclone S.p.A., Pavia, Italy) supplemented with 10% FBS (Euroclone S.p.A., Pavia, Italy), 100 U/ml penicillin and 100 μg/mL streptomycin (Sigma Aldrich S.r.l., Milano, Italy). NIH3T3 cells were maintained in DMEM High Glucose enriched with 10% FCS (Promocell, Heidelberg, Germany), 100 U/ml penicillin and 100 μg/mL streptomycin. Cultures were incubated at 37 °C in a humidified atmosphere.

Primary cultures of human umbilical vein endothelial cell (HUVEC) were obtained by enzymatic digestion of umbilical vein endothelial layer with a 0.1% collagenase IV solution (Sigma Aldrich, Milan, Italy). The cells were seeded on Petri dishes (BD, Franklin Lakes, NJ USA) previously coated with fibronectin (1 μg/mL; Sigma) and cultured with Endothelial Cell growth Medium MV$_2$ (basal medium, Promocell, Hidelberg, Germany) supplemented with 5% FCS, ascorbic acid (1 μg/mL), hFGF-2 (10 ng/mL), hEGF (5 ng/mL), hydrocortisone (0.2 μg/mL), R^3-IGF-1 (20 ng/mL), VEGF (0.5 ng/mL) (endothelial MV$_2$ medium kit, Promocell), and 1% antibiotic solution (Sigma), containing streptomycin sulfate (10 ng/mL), amphotericin-B (250 ng/mL) and penicillin G (100 U/mL). Cultures were incubated at 37 °C in a humidified atmosphere. The endothelial cells were used up to the fifth passage and harvested at 80% confluence.

4.3.3. Evaluation of anti-proliferative activity

Cells were seeded into a 96-well plate at the following cell density: 1.5×10^4 cell/cm^2 (A431), 6×10^3 cell/cm^2 (NIH3T3), 2.5×10^4 cell/cm^2 (MCF-7, HT-29, HeLa, BNL), and 1×10^4 cell/cm^2 (HUVECs). After a 24 h incubation period, media were replaced with ones containing or not various concentrations (ranging from 0.01 to 10 μM) of the tested compounds. After 20 h or 68 h incubation, cells were treated with 3-(4,5-dimethylthiazol-2-yl)-2,5-dimethyltetrazolium bromide (MTT) (0.50 mg/ml, Sigma) for 4 h. Formazan precipitates were dissolved in 2-propanol acid (0.04 M HCl in 2-propanol; Sigma) and optical density was measured at 570 nm, using a Microplate autoreader EL 13 (BIO-TEK instruments Inc., Winooski, Vermont USA). Results were expressed as IC_{50}, i.e. the concentrations of the agents (μM) which induced a 50% reduction of viability in comparison with non-treated cultures.

To verify the reversibility of the antiproliferative activity, HUVECs (1.5×10^4 cell/cm^2) were seeded into a 96-well plate. After a 24 h incubation period, cultures were treated with 10 μM of the tested compounds for 4 h. Media were removed and, after washing with phosphate buffer (PBS; Gibco-Invitrogen Corporation, Milano, Italy), cells were allowed to recover for 68 h in compound-free medium. To determine cell viability the (MTT)-tetrazolium dye assay was performed as described above. Results were expressed as percent change from control non-treated cultures.

The linearity of absorbance of formazan over a range of 5×10^3–5×10^5 cells was established by determining the linear coefficient (0.9799).

4.3.4. Evaluation of pro-apoptotic activity

HUVECs (2.5×10^4 cell/cm^2) were seeded into a 96-well plate and incubated at 37 °C for 24 h. Then, cultures were washed and treated with compounds (10 μM) for 24 h. Apoptosis was detected by an enzyme-linked immunoassorbent assay (ELISA) using the Cell Death Detection ELISA^{PLUS} Kit (Roche Diagnostics S.p.A., Monza, Italy) according to the manufacturer's instructions. Briefly, at the end of incubation period, cells were lysated and then centrifuged. Aliquots of supernatant were transferred to a streptavidin-coated well of a microtiter plate. Apoptosis detection was based on a quantitative sandwich-enzyme immunoassay using peroxidase-labeled monoclonal antibodies directed against DNA and histones of mono- and oligo-nucleosomes in supernatants of cell lysates. Peroxidase retained in immunocomplexes was measured photometrically at 405 nm wavelength using diammonium 2,2'-azino-bis(3-ethylbenzothiazoline-6-sulfonate) as substrate. Results were expressed as percent change from control non-treated cultures.

4.3.5. Cell migration

Cell migration was evaluated using a modified Boyden chamber. HUVECs (3×10^4 cell/cm^2) were seeded on the upper side of 5.0 μm pore Transwell insert (Corning Inc.) in basal medium supplemented with 1% FCS with or without noncytotoxic concentration of the tested compounds (1 μM). Inserts were placed in a 24-well plate containing medium supplemented with growth factors (lower chamber). After 4 h, cultures were fixed in 10% formaldehyde (Sigma) and the upper membrane of the insert was swabbed to remove non-migrated cells. The membrane was cut from the insert and mounted with DAPI. HUVEC migration was quantified by counting the number of nuclei in the lower side of the membrane in five random fields per insert (magnification ×100) by fluorescence microscopy. Experiments were repeated five times. Results were expressed as percent change from control cultures incubated with basal medium supplemented only with growth factors.

4.3.6. Morphogenesis assay

Morphogenesis analysis was carried out seeding HUVECs on Matrigel (BD Biosciences). Matrigel was thawed on ice overnight, spread evenly over each well (50 μL) of a 24-well plate, and allowed to polymerized for 30 min at 37 °C. HUVECs (2.5×10^4 cells/cm^2) were seeded on Matrigel and cultured in basal medium supplemented with 1% FCS, with or without not cytotoxic concentrations of the tested compounds (0.1 μM). Other wells were evenly coated with Matrigel GFR (Growth Factor Reduced). HUVECs (2.5×10^4 cells/cm^2) were seeded on Matrigel and cultured in basal medium supplemented with 1% FCS with or without not cytotoxic concentrations of the tested compounds (0.1 μM). After 18 h of incubation at 37 °C, cultures were fixed in 2% glutaraldehyde in cacodylate buffer, pH 7.2 and then photographed (5 fields for each well: the four quadrants and the center) at a magnification ×50. Phase contrast images were recorded using a digital camera and image analysis was carried out using the ImageJ image analysis software. The following dimensional

parameters (percent area covered by HUVECs and total length of HUVECs network per field) and topological parameters (number of meshes, and branching points per fields) were estimated. Values were expressed as percent change from control non-treated cultures.

4.3.7. In vivo antitumor activity

The *in vivo* antitumor activity of compounds **7**–**9** was evaluated in Balb/c mice using a syngenic murine hepatocellular carcinoma cell line (BNL 1ME A.7R.1) [43]. Briefly, male mice, 10 weeks old, were purchased from Harlan (S. Pietro al Natisone Udine, Italy), and 10^7 BNL 1ME A.7R.1 cells in 200 µL of sterile PBS were injected subcutaneously in the dorsal region. The animals were randomly divided into four groups, and starting on the seventh day, they were daily dosed intraperitoneally (ip) with 10 50 mg/kg body weight in vehicle (0.9% NaCl containing 5% polyethylene glycol 400 and 0.5% Tween 80), of either compound **7**, **8** or **9** or just vehicle. Tumor sizes were measured daily for 7 days using a pair of callipers and the tumor volume (V) was calculated by the rotational ellipsoid formula: $V = AB^2/2$, where A is the longer diameter (axial) and B is the shorter diameter (rotational). All experimental procedures followed guidelines recommended by the Institutional Animal Care and Use Committee of Padova University.

4.3.8. In vivo Matrigel plug assay

All experiments were performed according to D.L.G.S. 116/92 which warrants care of experimental animals in Italy. The research project was approved by the Italian Health Department according to the art. 7 of above mentioned D.L. Three-month-old C57/BL6 mice were anesthetized with isoflurane (2–3%) via nose cone and 100% oxygen used as carrier gas; the flank was shaved and disinfected with ethyl alcohol. A total of 0.5 mL of Matrigel GFR, mixed with 12 U.I. heparin (Vister) with or without 200 ng/plug FGF-2 and 1 µM tested compounds, was injected subcutaneously into the flank. After injection, the Matrigel polymerized forming a plug. After 7 days, the animals were sacrificed and the plugs were carefully removed and steeped in 300 µL/plug Brij-35 0.1% solution in PBS overnight at 4 °C. Hemoglobin concentration was analyzed using Drabkin's Reagent kit (Sigma). The optical density was read at 540 nm using a Microplate autoreader EL 13. The results were expressed as mg/m haemoglobin.

4.3.9. Statistical analysis

Unless otherwise indicated, the results are presented as the mean ± SEM. The differences between different treatments were analyzed using the two-sided Student's *t* test. *P* values of less than 0.05 were considered significant.

Acknowledgments

Appendix A. Supplementary data

Supplementary data related to this article can be found at http://dx.doi.org/10.1016/j.ejmech.2013.06.057.

References

[1] K. Collins, T. Jacks, N.P. Pavletich, The cell cycle and cancer, Proc. Natl. Acad. Sci. U. S. A. 94 (1997) 2776–2778.

[2] E. Zwick, J. Bange, A. Ullrich, Receptor tyrosine kinase signalling as a target for cancer intervention strategies, Endocr. Relat. Cancer 8 (2001) 161–173.

[3] A.C. Porter, R.R. Vaillancourt, Tyrosine kinase receptor-activated signal transduction pathways which lead to oncogenesis, Oncogene 17 (1998) 1343–1352.

[4] D.R. Robinson, Y.M. Wu, S.F. Lin, The protein tyrosine kinase family of the human genome, Oncogene 19 (2000) 5548–5557.

[5] J. Schlessinger, Cell signaling by receptor tyrosine kinases, Cell 103 (2000) 211–225.

[6] J. Baselga, J. Arribas, Treating cancer's kinase 'addiction', Nat. Med. 10 (2004) 786–787.

[7] A. Levitzki, A. Gazit, Tyrosine kinase inhibition: an approach to drug development, Science 267 (1995) 1782–1788.

[8] A. Petrelli, S. Giordano, From single- to multi-target drugs in cancer therapy: when aspecificity becomes an advantage, Curr. Med. Chem. 15 (2008) 422–432.

[9] J. Dowell, J.D. Minna, P. Kirkpatrick, Erlotinib hydrochloride, Nat. Rev. Drug Discov. 4 (2005) 13–14.

[10] M.H. Cohen, G.A. Williams, R. Sridhara, G. Chen, R. Pazdur, FDA drug approval summary: gefitinib (ZD1839) (Iressa) tablets, Oncologist 8 (2003) 303–306.

[11] E.R. Wood, A.T. Truesdale, O.B. McDonald, D. Yuan, A. Hassell, S.H. Dickerson, B. Ellis, C. Pennisi, E. Horne, K. Lackey, K.J. Alligood, D.W. Rusnak, T.M. Gilmer, L. Shewchuk, A unique structure for epidermal growth factor receptor bound to GW572016 (Lapatinib): relationships among protein conformation, inhibitor off-rate, and receptor activity in tumor cells, Cancer Res. 64 (2004) 6652–6659.

[12] A. Morabito, M.C. Piccirillo, F. Falasconi, G. De Feo, A. Del Giudice, J. Bryce, M. Di Maio, E. De Maio, N. Normanno, F. Perrone, Vandetanib (ZD6474), a dual inhibitor of vascular endothelial growth factor receptor (VEGFR) and epidermal growth factor receptor (EGFR) tyrosine kinases: current status and future directions, Oncologist 14 (2009) 378–390.

[13] D. Li, L. Ambrogio, T. Shimamura, S. Kubo, M. Takahashi, L.R. Chirieac, R.F. Padera, G.I. Shapiro, A. Baum, F. Himmelsbach, W.J. Rettig, M. Meyerson, F. Solca, H. Greulich, K.K. Wong, BIBW2992, an irreversible EGFR/HER2 inhibitor highly effective in preclinical lung cancer models, Oncogene 27 (2008) 4702–4711.

[14] C.M. Galmarini, Canertinib pfizer, IDrugs 7 (2004) 58–63.

[15] G. Marzaro, A. Guiotto, A. Chilin, Quinazoline derivatives as potential anticancer agents: a patent review (2007–2010), Expert Opin. Ther. Pat. 22 (2012) 223–252.

[16] A. Chilin, M.T. Conconi, G. Marzaro, A. Guiotto, L. Urbani, F. Tonus, P. Parnigotto, Exploring epidermal growth factor receptor (EGFR) inhibitor features: the role of fused dioxygenated rings on the quinazoline scaffold, J. Med. Chem. 53 (2010) 1862–1866.

[17] M.T. Conconi, G. Marzaro, A. Guiotto, L. Urbani, I. Zanusso, F. Tonus, M. Tommasini, P.P. Parnigotto, A. Chilin, New vandetanib analogs: fused tricyclic quinazolines with antiangiogenic potential, Invest. New Drugs 30 (2012) 594–603.

[18] G. Shen, Y. Hu, J. Wu, K. Jin, D. Zhu, Y. Zhang, Y. Yu, Y. Lou, A 2,6-disubstituted 4-anilinoquinazoline derivative facilitates cardiomyogenesis of embryonic stem cells, ChemMedChem 7 (2012) 733–740.

[19] H. Assefa, S. Kamath, J.K. Buolamwini, 3D-QSAR and docking studies on 4-anilinoquinazoline and 4-anilinoquinoline epidermal growth factor receptor (EGFR) tyrosine kinase inhibitors, J. Comput. Aided Mol. Des. 17 (2003) 475–493.

[20] J.J. Liao, Molecular recognition of protein kinase binding pockets for design of potent and selective kinase inhibitors, J. Med. Chem. 50 (2007) 409–424.

[21] A. Chilin, G. Marzaro, S. Zanatta, A. Guiotto, A microwave improvement in the synthesis of the quinazoline scaffold, Tetrahedron Lett. 48 (2007) 3229–3231.

[22] G. Marzaro, A. Guiotto, G. Pastorini, A. Chilin, A novel approach to quinazolin-4(3H)-one via quinazoline oxidation: an improved synthesis of 4-anilinoquinazolines, Tetrahedron 66 (2010) 962–968.

[23] G. Marzaro, A. Chilin, G. Pastorini, A. Guiotto, A novel convenient synthesis of benzoquinazolines, Org. Lett. 8 (2006) 255–256.

[24] A.J. Bridges, H. Zhou, D.R. Cody, G.W. Rewcastle, A. McMichael, H.D. Showalter, D.W. Fry, A.J. Kraker, W.A. Denny, Tyrosine kinase inhibitors. 8. An unusually steep structure–activity relationship for analogues of 4-(3-bromoanilino)-6,7-dimethoxyquinazoline (PD 153035), a potent inhibitor of the epidermal growth factor receptor, J. Med. Chem. 39 (1996) 267–276.

[25] J. Folkman, P. Cole, S. Zimmerman, Tumor behavior in isolated perfused organs: in vitro growth and metastases of biopsy material in rabbit thyroid and canine intestinal segment, Ann. Surg. 164 (1966) 491–502.

[26] N. Ferrara, R.S. Kerbel, Angiogenesis as a therapeutic target, Nature 438 (2005) 967–974.

[27] C. Michiels, T. Arnould, J. Remacle, Endothelial cell responses to hypoxia: initiation of a cascade of cellular interactions, Biochim. Biophys. Acta 1497 (2000) 1–10.

[28] B. Hobson, J. Denekamp, Endothelial proliferation in tumours and normal tissues: continuous labelling studies, Br. J. Cancer 49 (1984) 405–413.

[29] P. Carmeliet, R.K. Jain, Angiogenesis in cancer and other diseases, Nature 407 (2000) 249–257.

[30] V. Levina, Y. Su, B. Nolen, X. Liu, Y. Gordin, M. Lee, A. Lokshin, E. Gorelik, Chemotherapeutic drugs and human tumor cells cytokine network, Int. J. Cancer 123 (2008) 2031–2040.

[31] C.H. Heldin, B. Westermark, Mechanism of action and in vivo role of platelet-derived growth factor, Physiol. Rev. 79 (1999) 1283–1316.

[32] F. Anselmi, M. Orlandini, M. Rocchigiani, C. De Clemente, A. Salameh, C. Lentucci, S. Oliviero, F. Galvagni, c-ABL modulates MAP kinases activation downstream of VEGFR-2 signaling by direct phosphorylation of the adaptor proteins GRB2 and NCK1, Angiogenesis 15 (2012) 187–197.

[33] G. Hu, A.T. Place, R.D. Minshall, Regulation of endothelial permeability by Src kinase signaling: vascular leakage versus transcellular transport of drugs and macromolecules, Chem. Biol. Interact. 171 (2008) 177–189.

[34] J.T. Parsons, S.J. Parsons, Src family protein tyrosine kinases: cooperating with growth factor and adhesion signaling pathways, Curr. Opin. Cell Biol. 9 (1997) 187–192.

[35] D. Srinivasan, R. Plattner, Activation of Abl tyrosine kinases promotes invasion of aggressive breast cancer cells, Cancer Res. 66 (2006) 5648–5655.

[36] M. Al-Otaiby, E. Tassi, M.O. Schmidt, C.D. Chien, T. Baker, A.G. Salas, J. Xu, M. Furlong, R. Schlegel, A.T. Riegel, A. Wellstein, Role of the nuclear receptor coactivator AIB1/SRC-3 in angiogenesis and wound healing, Am. J. Pathol. 180 (2012) 1474–1484.

[37] R. Gupta, M.L. Maitland, Sunitinib, hypertension, and heart failure: a model for kinase inhibitor-mediated cardiotoxicity, Curr. Hypertens. Rep. 13 (2011) 430–435.

[38] E.F. Pettersen, T.D. Goddard, C.C. Huang, G.S. Couch, D.M. Greenblatt, E.C. Meng, T.E. Ferrin, UCSF Chimera—a visualization system for exploratory research and analysis, J. Comput. Chem. 25 (2004) 1605–1612.

[39] Marvin, Version 5.5.0.1, Program B; ChemAxon: Budapest, Hungary; www.chemaxon.com/products.

[40] N.M. O'Boyle, M. Banck, C.A. James, C. Morley, T. Vandermeersch, G.R. Hutchison, Open Babel: an open chemical toolbox, J. Cheminf. 3 (2011) 33.

[41] G.M. Morris, R. Huey, W. Lindstrom, M.F. Sanner, R.K. Belew, D.S. Goodsell, A.J. Olson, AutoDock4 and AutoDockTools4: automated docking with selective receptor flexibility, J. Comput. Chem. 30 (2009) 2785–2791.

[42] Y. Koyama, T. Barrett, Y. Hama, G. Ravizzini, P.L. Choyke, H. Kobayashi, In vivo molecular imaging to diagnose and subtype tumors through receptor-targeted optically labeled monoclonal antibodies, Neoplasia 9 (2007) 1021–1029.

[43] V. Gasparotto, I. Castagliuolo, G. Chiarelotto, V. Pezzi, D. Montanaro, P. Brun, G. Palu, G. Viola, M.G. Ferlin, Synthesis and biological activity of 7-phenyl-6,9-dihydro-3H-pyrrolo[3,2-*f*]quinolin-9-ones: a new class of antimitotic agents devoid of aromatase activity, J. Med. Chem. 49 (2006) 1910–1915.